

## AN X-RAY COOLING-CORE CLUSTER SURROUNDING A LOW POWER COMPACT STEEP SPECTRUM RADIO SOURCE 1321+045

M. KUNERT-BAJRASZEWSKA<sup>1</sup>, A. SIEMIGINOWSKA<sup>2</sup>, A. LABIANO<sup>3</sup>

<sup>1</sup> Toruń Centre for Astronomy, Faculty of Physics, Astronomy and Informatics, NCU, Grudziacka 5, 87-100 Toruń, Poland

<sup>2</sup> Harvard Smithsonian Center for Astrophysics, 60 Garden St, Cambridge, MA 02138 and

<sup>3</sup> Centro de Astrobiología (CSIC-INTA), Carretera de Ajalvir km. 4, 28850 Torrejon de Ardoz, Madrid, Spain

Draft version May 30, 2018

### ABSTRACT

We discovered an X-ray cluster in a *Chandra* observation of the compact steep spectrum (CSS) radio source 1321+045 ( $z = 0.263$ ). CSS sources are thought to be young radio objects at the beginning of their evolution and can potentially test the cluster heating process. 1321+045 is a relatively low luminosity source and its morphology consists of two radio lobes on the opposite sides of a radio core with no evidence for jets or hotspots. The optical emission line ratios are consistent with an interstellar medium (ISM) dominated by AGN-photoionization with a small contribution from star formation, and no contributions from shocks. Based on these ratios, we classify 1321+045 as a low excitation galaxy (LEG) and suggest that its radio activity is in a coasting phase. The X-ray emission associated with the radio source is detected with  $36.1 \pm 8.3$  counts, but the origin of this emission is highly uncertain. The current X-ray image of the cluster does not show any signatures of a radio source impact on the cluster medium. *Chandra* detects the cluster emission at  $> 3\sigma$  level out to  $\sim 60''$  (240 kpc). We obtain the best fit beta model parameters of the surface brightness profile of  $\beta = 0.58 \pm 0.2$  and a core radius of  $9.4_{-0.9}^{+1.1}$  arcsec. The average temperature of the cluster is equal to  $kT = 4.4_{-0.3}^{+0.5}$  keV, with a temperature and cooling profile indicative of a cooling core. We measure the cluster luminosity  $L_{(0.5-2\text{keV})} = 3 \times 10^{44}$  erg s<sup>-1</sup> and mass  $1.5 \times 10^{14} M_{\odot}$ .

*Keywords:* active — galaxies: jets — X-rays: galaxies; clusters

### 1. INTRODUCTION

Many X-ray clusters are found around radio galaxies with large-scale radio structures which in majority are classified as FR Is (Fanaroff & Riley 1974) with a smaller number of FR IIs (Owen & Ledlow 1997). These radio sources are old ( $> 10^7$  years) and their long term interaction with the cluster environment imprinted a rich variety of structures into the X-ray morphology, such as bubbles, shock fronts and ripples (McNamara & Nulsen 2007; Fabian 2012). However, little is known about the nature of the X-ray clusters associated with young compact radio sources (with radio source sizes  $< 20$  kpc), namely the Gigahertz Peaked Spectrum (GPS) and Compact Steep Spectrum (CSS) objects. These young (age  $< 10^5$  years) radio sources are believed to be at the beginning of their evolution (Readhead et al. 1996; Fanti et al. 1995). If they reside in clusters the inter-cluster medium (ICM) should have not been impacted by the radio source and we could observe a primordial X-ray morphology of the cluster medium. In addition the observation of the cluster medium can provide important information about the physical properties and evolution of the radio source itself. However, searches for luminous X-ray clusters associated with GPS and CSS objects were typically unsuccessful (Siemiginowska et al. 2003, 2008).

The only bright X-ray cluster known to host a CSS source is 3C186 discovered by Siemiginowska et al. (2005, 2010). It is a well formed cool core X-ray cluster at high redshift,  $z = 1.06$ . The central cluster galaxy hosts a radio-loud quasar with a powerful FR II-type small-scale radio morphology indicating the initial phase of its evolution. While expanding into the cluster medium,

the young radio source can potentially supply the energy required to stabilize the cluster core against catastrophic cooling. However, the high redshift location of this source limits the investigation of the interactions between the radio source and the ICM.

We discovered an X-ray emission from the galaxy cluster, MaxBCG J201.08197+04.31863 (Koester et al. 2007) in our *Chandra* observation of a low power CSS radio source, 1321+045 at  $z = 0.263$ . Here, we present the analysis of the X-ray cluster emission together with the analysis of the radio, optical and X-ray properties of the radio source 1321+045. This is the second CSS source known to be associated with the large X-ray cluster. It has a different radio morphology than the 3C186 (FR I vs. FR II-like) and it is much less luminous in radio. These two CSS sources probe different radio source properties but in a similar cluster environment.

Throughout the paper, we assume the cosmology with  $H_0 = 71$  km s<sup>-1</sup> Mpc<sup>-1</sup>,  $\Omega_M = 0.27$ ,  $\Omega_{\Lambda} = 0.73$ .

### 2. THE CHANDRA X-RAY OBSERVATIONS AND DATA ANALYSIS

The *Chandra* ACIS-S observation of 1321+045 was part of a small snapshot program targeting seven low radio power CSS sources (in preparation). It was performed on 2011-12-14. The source was placed at the aim point on the back-illuminated ACIS CCD (S3) and the observation was made in FAINT mode with 1/8 CCD readout to avoid pileup. We used CIAO 4.4 (Fruscione et al. 2006) and CALDB 4.5 in all the data analysis and *Sherpa* (Freeman et al. 2001) for modeling and fitting (`cstat` with `simplex` method). We reprocessed the data using `chandra_repro` to apply the

**Table 1**  
Best Fit Model Parameters for the X-ray cluster<sup>a</sup>

R <sup>b</sup> (arcsec)	Range (arcsec)	Total Counts <sup>c</sup>	Net Counts <sup>c</sup>	kT <sup>d</sup> (keV)	Norm <sup>e</sup>	n <sub>e</sub> (10 <sup>-2</sup> cm <sup>-3</sup> )	S <sup>f</sup> (keV cm <sup>-2</sup> )	t <sup>g</sup> (10 <sup>9</sup> yrs)
5.3	2.0-8.6	815.0±28.5	761.5±29.5	3.9 <sup>+0.7</sup> <sub>-0.6</sub>	0.0186±0.0012	3.9±0.6	33.9±6.6	1.6±0.3
11.9	8.6-15.2	696.0±26.4	575.9±28.5	4.1 <sup>+0.9</sup> <sub>-0.7</sub>	0.0043±0.0003	1.9±0.4	57.6±13.8	3.3±0.8
21.8	15.2-28.4	924.0±30.4	606.4±35.2	5.4 <sup>+0.6</sup> <sub>-0.5</sub>	0.0014±0.0001	1.1±0.1	109.2±12.9	6.7±0.7

<sup>a</sup> listed uncertainties are at 68% for one interesting parameter. <sup>b</sup> The assumed annuli are circular with the mean radius listed in the R column and ranges in Range column; <sup>c</sup> A number of counts within the 0.5-7 keV energy range. <sup>d</sup> deprojected temperature; <sup>e</sup> Normalization for APEC thermal model defined as Norm =  $\frac{10^{-14}}{4\pi[D_A(1+z)]^2} \int n_e n_H dV$  with the abundance table set to Anders & Grevesse (1989); Note that the Norm values given by **deproject** are normalized to a total volume given by the outermost sphere. <sup>f</sup> Entropy; <sup>g</sup> cooling time.

most recent instrument calibration. The script runs `acis_process_events` which applies the sub-pixel algorithm and gives the best spatial resolution images. After the standard deadtime correction of 9.4% the effective exposure time on the source was 9.5 ksec. The X-ray centroid is located at R.A. = 13<sup>h</sup>24<sup>m</sup>19<sup>s</sup>.646, Decl. = +4°19′07″.45 (J2000.0).

### 2.1. Image Analysis

The X-ray diffuse emission covers a large part of the ACIS-S CCD with the radio source located in the center (Figure 1). The smoothed X-ray image overlaid with radio contours shown in Fig. 1 seems to suggest a broad enhanced X-ray emission with two peaks in the vicinity of the core. Offsets between the radio core and the enhancements are consistent with the astrometric uncertainty of *Chandra* and we did not attempt to apply any additional adjustments. The adjustment to the aspect solution might be possible with a deeper observations in the future if there are additional point sources detected in this field.

The X-ray cluster emission extends outside the field of view of the CCD. However, we measured the extent along the CCD using the surface brightness profiles towards the north and south from the center. We used `dmextract` and extracted one-dimensional radial profiles assuming 18 annuli located between 3″ and 100″ within PA angles of 70°-150° and 260°-335°. The cluster emission is detected at 3σ level out to about ~60″ (~240 kpc) from the radio source. We fit the two profiles in *Sherpa* assuming a `beta1d` model and obtained the core radius of  $r_c = 9.4^{+1.1}_{-0.9}$  arcsec and β-parameter of  $0.58^{+0.03}_{-0.02}$ . The extrapolation of the beta1d model into the circular ( $r = 2″$ ) region centered on the radio source shows the excess X-ray emission. We associate this emission with the radio source.

### 2.2. An X-ray emission from the radio core

We used `specextract` tool to extract the X-ray spectra assuming 1.25″ radius circle for the radio source and an annulus with inner and outer radii equal to 1.5″ and 10″ respectively for the local background. This region encloses the radio core and a part of the innermost radio structure. The X-ray spectrum contains 36.1±8.3 net counts (53 total) in the 0.5-7 keV energy range. The cluster emission contributes to this spectrum and we need to take it into account in the further modeling of the source spectrum. In the modeling we kept the absorption parameter at the Galactic value of  $N_H = 2.04 \times 10^{20} \text{ cm}^{-2}$  (Dickey & Lockman 1990).

We first fit the background spectrum assuming the APEC model in *Sherpa* (this is the cluster emission within 1.5″ and 10″ annulus). We set the metal abun-

dance to 30% of the Solar values and  $z = 0.263$  for this model and fit the spectrum containing 1054 counts in 0.5-7 keV range. The resulting best fit temperature and normalization are  $kT_b = 4.4^{+0.5}_{-0.3}$  keV and  $8.8 \pm 0.3 \times 10^{-4}$  respectively and represent the average observed values of the central region of the cluster. We expect only about 16±4 counts from the cluster to contribute to the *Chandra* spectrum of the radio source. These background model parameters remained unchanged in fitting the spectrum of the radio source described below.

We assumed an absorbed powerlaw emission model for the radio source and the APEC model with the fixed parameters to the above best fit values to account for the cluster emission. The resulting best fit power law photon index is equal to  $\Gamma = 2.35^{+0.39}_{-0.36}$  and the normalization to  $6.2^{+1.4}_{-1.2} \times 10^{-6}$  photons cm<sup>2</sup> s<sup>-1</sup> at 1 keV. The model unabsorbed flux of  $F_{0.5-2 \text{ keV}} = 1.4 \pm 0.3 \times 10^{-14}$  erg cm<sup>-2</sup> s<sup>-1</sup> corresponds to the luminosity  $L_{X(0.5-2 \text{ keV})} \sim 3 \times 10^{42}$  erg s<sup>-1</sup> typical for a low luminosity AGN. The photon index, however, is quite steep and may indicate a presence of soft thermal emission often observed in low luminosity AGN and explained as a result of hot ISM of the host galaxy or a jet emission (Hardcastle et al. 2009; LaMassa et al. 2012). A higher quality spectrum is needed to understand the origin of this emission.

### 2.3. Spectral analysis of the X-ray cluster

We detected 2882.2±55.4 net counts within the circular region with 38.2″ radius in the *Chandra* 9.7 ksec observation. The cluster is bright in X-rays and we attempted to obtain the cluster’s temperature profile by fitting the spectra of three annuli centered on the radio source. The three annuli span the cluster emission between 2″ and 28″ and the fourth one between 28″ and 35″ accounts for the background (see Table 1).

We assume the APEC model and fit the cluster spectrum in each annulus. We account for the cluster 3D volume effects using the `deproject` model in *Sherpa* (for model details see Fabian et al. 1981; Kriss et al. 1983; Siemiginowska et al. 2010). The best-fit model provides the cluster temperatures, normalizations, and densities listed in Table 1.

These numbers suggest that the cluster has a cooling core, although this result has to be confirmed with better quality data in the future. We used the exposure corrected image given by `fluximage` tool and assumed an elliptical region with 35″ and 60″ radii to estimate the X-ray luminosity of the cluster to be  $L_{(0.5-2 \text{ keV})} = 3 \times 10^{44}$  erg s<sup>-1</sup>. The mass of the cluster enclosed by a sphere with 60″ radius is about  $1.5 \times 10^{14} M_\odot$  assuming the average cluster temperature of 4.4 keV, and  $\beta = 0.58$ ,

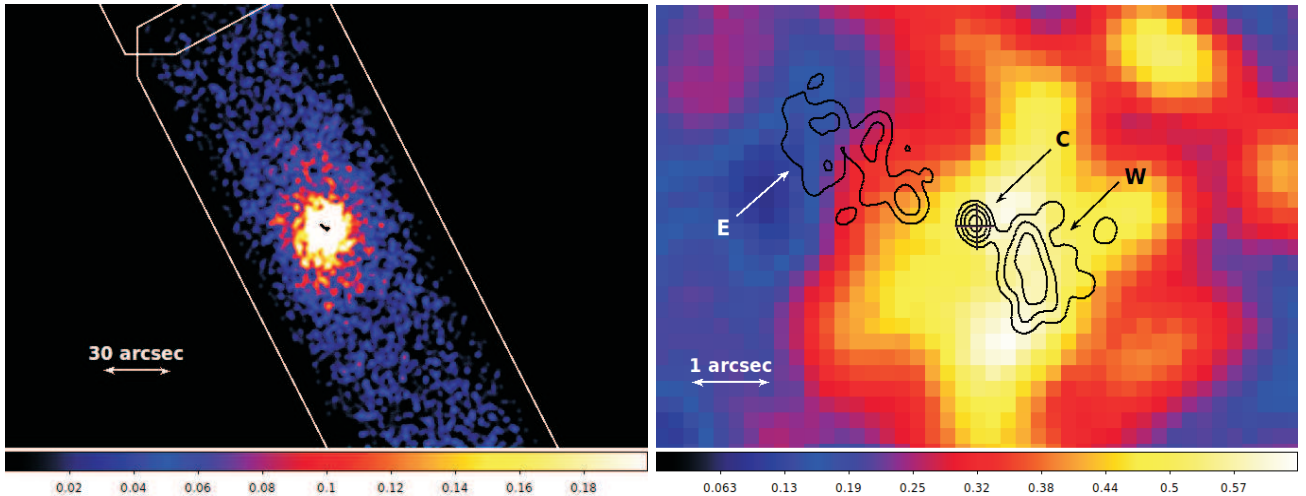


**Figure 1.** *Chandra* ACIS-S X-ray image in 0.5-7 keV energy range overlaid with the black radio contours from the MERLIN 1.6 GHz image. The radio contours increase by factor of 2, the first contour level corresponds to  $\approx 3\sigma$  and amounts 0.8 mJy/beam. (Left) The X-ray image smoothed with the Gaussian function ( $\sigma=2$  arcsec). A  $30''$  scale bar corresponds to  $\sim 121$  kpc. The white contours indicate the exposed part of the CCD detector. (Right): The central region of the cluster showing the ACIS-S image smoothed with the Gaussian function ( $\sigma=0.98$  arcsec), the radio contours and the optical SDSS source (black cross). The  $1''$  scale bar corresponds to  $\sim 4$  kpc. The radio lobes (E,W) and the core (C) are marked.

which is in a broad agreement with the clusters scaling relations in Eckmiller et al. (2011).

### 3. DISCUSSION AND CONCLUSIONS

#### 3.1. Low Power Radio Source

The radio source 1321+045 (R.A. =  $13^{\text{h}}24^{\text{m}}19^{\text{s}}.7$ , Decl. =  $+04^{\circ}19'07.2''$  (J2000.0)) belongs to a class of young CSS radio sources (Fanti et al. 1995). It has been observed with MERLIN at 1.6 GHz in 2007 as a part of large sample of low luminosity compact (LLC) sources (Kunert-Bajraszewska et al. 2010a). The position of the central component visible in 1.6 GHz MERLIN image is well correlated with the position of the optical counterpart suggesting it is a radio core (C). The two lobes (E and W) are located on the opposite sides of the core. There is no evidence of jets or hotspots, however, this needs to be confirmed by observations at higher frequency. A total projected length of the source is equal to  $\sim 17$  kpc and its radio luminosity,  $L_{5\text{GHz}} \sim 10^{25} \text{ W Hz}^{-1}$  ( $< 10^{42} \text{ erg s}^{-1}$ ), places it in the FRI-FRII transition region.

Studies of compact radio sources suggest that they exhibit periodic activity on timescales of  $10^4 - 10^5$  years (Reynolds & Begelman 1997). On shorter timescales the radio source is not able to escape from the host galaxy and starts to recollapse within the ISM (Czerny et al. 2009). Our analysis of the whole sample of LLC sources suggest that they can represent a population of short-lived objects and undergo this phase of activity many times before they become large scale FRI or FRII (Kunert-Bajraszewska et al. 2010a,b). What is more, the evolution of the radio source and its radio morphology is determined by the properties of the central engine: strength, accretion mode, excitation level of the ionized gas, and the ISM. Optically many of them belong to the class of low excitation galaxies (LEGs), which are thought to be powered by the accretion of hot gas (Hardcastle et al. 2007; Buttiglione et al. 2010) and can be progenitors of large scale LEGs (Kunert-Bajraszewska et al.

2010b). The Ninth SDSS Data Release (Ahn et al. 2012) gives the fluxes of the emission lines visible in spectrum of 1321+045 and the calculated line ratios  $\log [\text{O II}]\lambda\lambda 3727, 3729 / [\text{O III}]\lambda 5007 = 1.15$  and  $\log [\text{O III}]\lambda 5007 / \text{H}\beta = -0.41$  (see Buttiglione et al. 2010, for definitions) are consistent with 1321+045 being a LEG.

We used ITERA (Groves & Allen 2010) to generate emission-line diagnostic (or BPT, after Baldwin et al. (1981)) diagrams and to compare the emission-line ratios of 1321+045 with predictions for starburst (Leitherer et al. 1999; Dopita et al. 2006; Levesque et al. 2010), dusty and dust-free AGN (Groves et al. 2004a), and shock (Allen et al. 2008) models. We found that the emission line ratios of 1312+045 are consistent with AGN-dominated photoionization with small contributions from star-formation models. None of the shock models (with and without precursor) reproduce the flux ratios, suggesting that jet-induced shocks are not present in the ISM of 1321+045 or their contribution to the ionization of the optically emitting gas is negligible.

#### 3.2. Interactions between the Radio Source and the ICM

The presence of distortions and cavities in the X-ray image of a cluster can signal interactions between the central galaxy (the radio source) and the ICM (Hlavacek-Larrondo et al. 2012). Some clusters have multiple pairs of cavities filled with low frequency radio emission, probably caused by the previous radio activity phase. The high resolution radio observations show that the reborn radio source can reside inside the cluster core and multiple cavities provide the evidence for the previous outbursts (O'Sullivan et al. 2012; Clarke et al. 2009; Tremblay et al. 2012). Figure 1 shows X-ray emission from the 1321+045 cluster in 0.5-7 keV energy range overlaid with radio contours from the MERLIN 1.6 GHz observations. There is no presence of any ripples and discontinuities in the current X-ray image of a 1321+045 cluster but rather uniform emission without indications of an interaction with the radio jets, or any signature of the previous activity.

Inspection of the VLSS image of 1321+045 at 74 MHz

(Cohen et al. 2007) shows that the low frequency emission extends out to  $\sim 120$  kpc. This low frequency radio emission is uniform and there is no trace of more extended components which could indicate the older phase of radio activity.

The synchrotron spectrum of 1321+045 consist of four points and is steep from 74 MHz to 5 GHz with the index  $\alpha = 0.95$  (defined as  $S \propto \nu^{-\alpha}$ ). We used a simple model of synchrotron emission (Kunert-Bajraszewska et al. 2009) to reproduce the observed spectrum in order to find the value of the magnetic field. We took the size of the radio lobe, assumed an equipartition between the particle energy and the magnetic field energy and a value of the Doppler factor  $\delta = 1$ . We obtained the best fit value of  $B = 1.5 \times 10^{-4}$  G which gives the magnetic pressure in each radio lobe to be  $\sim 9 \times 10^{-10}$  dyn cm $^{-2}$ . Based on the cluster central density and temperature we estimate a central thermal pressure of  $\sim 5 \times 10^{-10}$  dyn cm $^{-2}$ . Taking into account the uncertainties in determining the deprojected temperature and density (only three annuli) and the value of the thermal pressure we conclude that the cluster environment could limit the growth of the weak radio source.

Given the value of the magnetic field and the spectrum break frequency,  $\nu_{br}$  we can estimate the synchrotron age of the source 1321+045. The break frequency indicates the critical point in which the radio spectrum changes its spectral index and the value of  $\nu_{br}$  depends on the elapsed time since the source formation (Murgia et al. 1999). In the case of older objects the break frequency is moved toward lower frequencies. The synchrotron spectrum of 1321+045 does not show the self-absorption peak or the break frequency in the range 74 MHz–5 GHz. We suggest that the well-known electron self-absorption process modifies the index of the synchrotron emission of 1321+045 below the 74 MHz. However, since this assumption is based on a small number of spectral points we consider two cases in our calculation of the spectral age of the source: the break frequency is higher than 5 GHz or lower than 74 MHz. This gives us a synchrotron age of 1321+045 in the order of  $\sim 10^5$  and  $\sim 10^6$  years, respectively. The  $\nu_{br}$  lower than 74 MHz indicates that the population of electrons has cooled down to low energies and the source after a typical for CSS sources lifetime ( $10^4 - 10^5$  years) started to fade away. As we already suggested the evolutionary paths of young radio AGNs are probably determined by the properties of their central engines, namely the HEG/LEG path (Kunert-Bajraszewska et al. 2010b). However, in some objects the surrounding environment could be also an important factor influencing the evolution.

#### 4. SUMMARY

1321+045 is the first low power CSS LEG with FRI-like radio morphology discovered to be embedded in an X-ray cluster. The other CSS source, 3C186 (Siemiginowska et al. 2005, 2010) has powerful jets and hotspots that are characteristic of FR IIs. The radio observations of 1321+045 show a weak radio core and a symmetric diffuse emission from radio lobes without any compact features. There are no distortions and cavities in our current X-ray image of the cluster and deeper *Chandra* observations are required to confirm this result. The optical analysis rule out the presence of jet-induced

shocks in the ISM of 1321+045. We speculate that this low power small scale radio galaxy did not have enough energy to get out of the host galaxy and it is now in a coasting phase.

#### 5. ACKNOWLEDGMENTS

This research has made use of data obtained by the Chandra X-ray Observatory, and *Chandra* X-ray Center (CXC) in the application packages CIAO, ChIPS, and Sherpa. This research is funded in part by NASA contract NAS8-03060. Partial support for this work was provided by the *Chandra* grants GO1-12124X.

#### REFERENCES

- Ahn, C.P., et al., 2012, ApJS, 203, 21  
 Allen, M. G., et al., 2008, ApJS, 178, 20.  
 Anders E. & Grevesse N. 1989, GeCoA, 53, 197  
 Baldwin, J. A., Phillips, M.M., Terlevich, R., 1981, PASP, 93, 5  
 Buttiglione S., Capetti, A., Celotti, A., et al., 2010, A&A, 509, 6  
 Clarke, T.E., Blanton, E.L.; Sarazin, C.L., et al., 2009, ApJ, 697, 1481  
 Cohen, A.S., Lane, W.M., Cotton, W.D., et al., 2007, AJ, 134, 1245  
 Czerny B., Siemiginowska, A., Janiuk, et al., 2009, ApJ, 698, 840  
 Dickey, J. M., & Lockman, F. J. 1990, ARA&A, 28, 215  
 Dopita, M. A., Fischera, J., Sutherland, R. S., et al., 2006, ApJS, 167, 177.  
 Eckmiller, H. J., Hudson, D. S., & Reiprich, T. H. 2011, A&A, 535, A105  
 Fabian, A. C., Hu, E. M., Cowie, L. L., & Grindlay, J. 1981, ApJ, 248, 47  
 Fabian, A. C., 2012, ARA&A, 50, 455  
 Fanaroff, B. L., & Riley, J. M., 1974, MNRAS, 167, 31P  
 Fanti, C., Fanti, R., Dallacasa, D., et al., 1995, A&A 302, 317  
 Freeman, P., Doe, S., & Siemiginowska, A. 2001, SPIE, 4477, 76  
 Fruscione, A., et al. 2006, SPIE, 6270,  
 Groves, B. A & Allen, M. G, 2010, NewA, 15, 614  
 Groves, B. A., Dopita, M. A., Sutherland, R. S., 2004, ApJS, 153, 9  
 Hardcastle, M. J., Evans, D. A., Croston, J. H., 2007, MNRAS, 376, 1849  
 Hardcastle, M. J., Evans, D. A., & Croston, J. H. 2009, MNRAS, 396, 1929  
 Hlavacek-Larrondo, J., Fabian, A. C., Sanders, J. S., Taylor, G. B., 2012, MNRAS, 415, 3520  
 Kunert-Bajraszewska, M., Siemiginowska, A., Katarzyski, K., Janiuk, A., 2009, ApJ, 705, 1356  
 Kunert-Bajraszewska, M., Gawronski, M.P., Labiano A., Siemiginowska A., 2010a, MNRAS, 408, 2261  
 Kunert-Bajraszewska, M., & Labiano, A., 2010b, MNRAS, 408, 2279  
 Koester, B. P., McKay, T. A., Annis, J., et al. 2007, ApJ, 660, 239  
 Kriss, G. A., Cioffi, D. F., & Canizares, C. R. 1983, ApJ, 272, 439  
 LaMassa, S. M., Heckman, T. M., & Ptak, A. 2012, ApJ, 758, 82  
 Leatherer, C., et al., 1999, ApJS, 123, 3  
 Levesque, E. M., Kewley, L. J., Larson, K. L., 2010, AJ, 139, 712  
 McNamara, B. & Nulsen 2007, ARAA, 45, 117  
 Murgia, M., Fanti, C., Fanti, R., et al., 1999, A&A, 345, 769  
 O’Sullivan, E., Giacintucci, S., Babul, A., et al., 2012, MNRAS, 424, 2971  
 Owen, F. N., & Ledlow, M. J. 1997, ApJS, 108, 41  
 Readhead, A. C. S., Taylor, G. B., Xu, W., et al., 1996, ApJ 460, 612  
 Reynolds, C. S., & Begelman, M. C., 1997, ApJ, 487, L135  
 Siemiginowska, A., Aldcroft, T. L., Bechtold, J., et al. 2003, PASA, 20, 113  
 Siemiginowska, A., Cheung, C. C., LaMassa, S., 2005, ApJ, 632, 110  
 Siemiginowska, A., LaMassa, S., Aldcroft, T. L., et al., 2008, ApJ, 684, 811  
 Siemiginowska, A., Burke, D. J., Aldcroft, T. L., et al., 2010, ApJ, 722, 102  
 Tremblay, G. R., O’Dea, C. P., Baum, S. A., et al., 2012, MNRAS, 424, 1026